NANO LETTERS

2007
Vol. 7, No. 10
3177−3181

Material-Specific Infrared Recognition of Single Sub-10 nm Particles by Substrate-Enhanced Scattering-Type Near-Field Microscopy

A. Cvitkovic, N. Ocelic, and R. Hillenbrand*

Nano-Photonics Group, Max-Planck-Institut für Biochemie & Center for NanoScience (CeNS), 82152 Martinsried, Germany

Received July 21, 2007; Revised Manuscript Received August 27, 2007

ABSTRACT

We study the optical material contrast of single nanoparticles in infrared scattering-type near-field optical microscopy (IR s-SNOM) in the presence of strong probe–substrate coupling. It is shown theoretically and experimentally that the contrast depends on both the dielectric properties of the nanoparticles and on their size. We can separate the two dependencies by correlating the simultaneously acquired topography and near-field images pixel-by-pixel. This allows us to establish material-specific mapping of polydisperse nanoparticle mixtures with nanoscale spatial resolution. We experimentally demonstrate the differentiation between sub-10 nm gold and polymer particles adsorbed on a Si substrate. Possible applications of our method range from the material-specific mapping of nanoparticle assemblies to the measurement of the doping concentration in single semiconductor nanoparticles.

The detection and mapping of nanoparticles and clusters is a central issue in many fields of nano-, material, and biosciences. Knowledge about their distribution, chemical identity, or doping is vitally important for many applications ranging from characterization of nanocomposite materials to biolabeling. Among different analytical techniques, optical methods offer the advantage of being fast, noninvasive, and highly sensitive to widely different material properties such as chemical composition or conductivity. While the far-field optical detection of particles even smaller than 5 nm has already been demonstrated,[1−4] the spatial resolution is limited by diffraction to about half the illumination wavelength. This prevents material-specific single-particle mapping in dense nanoparticle assemblies or in complex hybrid systems. A possible solution is provided by tip-enhanced near-field optical microscopy, where optical antennas[5−7] such as metal particles[8−10] and tips[11−16] focus light to nanoscale dimensions. Although these methods have been successfully applied for nanoscale-resolved spectroscopic mapping of single carbon nanotubes,[17] tobacco mosaic viruses,[18] and molecules,[19−21] they generally suffer from weak scattering signals. As recently reported,[19,20,22] a significant signal enhancement can be achieved by strong near-field coupling between the probing tip and metallic or highly reflecting substrates. Here we study how the strong tip−substrate coupling in scattering-type near-field optical microscopy (substrate-enhanced s-SNOM[22]) affects the material-specific contrast of single nanoparticles smaller than the tip size (typically ≈10−20 nm radius). We observe that the near-field optical nanoparticle contrast depends on both the dielectric properties of the particles and their size, which is different from former reports[23−27] dealing with extended nanostructures. We analyze this effect and demonstrate that material- and size-dependent contrast can be separated. This allows us to establish material-specific optical mapping of polydisperse nanoparticle mixtures by s-SNOM. Particularly, we succeeded in the optical recognition of sub-10 nm gold and polymer particles within a mixture of particles adsorbed on a Si substrate with a spatial resolution of about 30 nm at a mid-infrared wavelength of about $\lambda = 10.6\ \mu$m.

Near-field optical imaging by s-SNOM[14] is performed by recording the light scattered from a sharp scanning probe such as a cantilevered atomic force microscope (AFM) tip simultaneously with the topography (Figure 1a). Vertical tip oscillation at a frequency Ω, interferometric detection and demodulation of the detector signal at a higher harmonic $n\Omega$ thereby allow an efficient background suppression. When the illuminated tip is located above a homogeneous flat sample surface, the scattered light and thus the near-field optical image contrast can be explained by approximating the probe by a dipole p_t located in the center of the tip apex.[24,28,29] Because of the near-field interaction between p_t

* Corresponding author. E-mail: hillenbr@biochem.mpg.de. Fax: +49 89 8578 2641.

10.1021/nl071775+ CCC: $37.00
Published on Web 09/20/2007

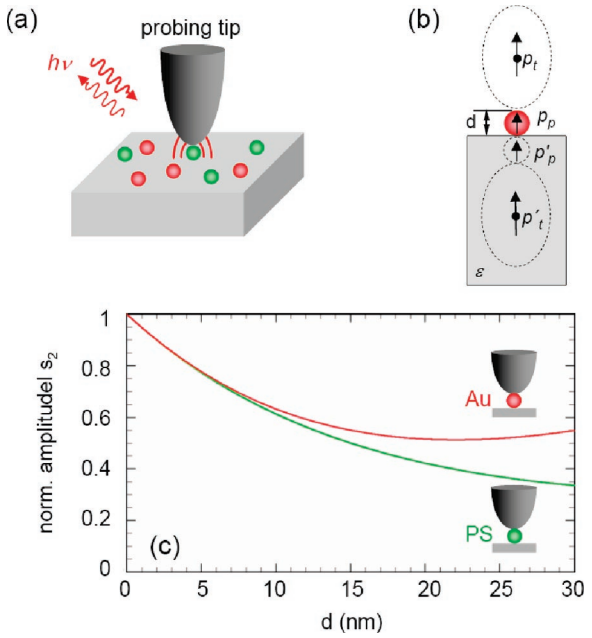

Figure 1. Material-specific recognition of sub-10 nm nanoparticles by substrate-enhanced s-SNOM. (a) Schematics of the experimental setup. (b) Illustration of the extended dipole model used for calculating the s-SNOM signals in (c). (c) Optical signal amplitude s_2 shown as a function of the particle diameter d, calculated for Au (red line) and PS nanoparticles (green line) on a Si substrate. All values are normalized to $s_2(d = 0)$. The calculation assumes a tip vibration amplitude of 20 nm and a second harmonic signal demodulation ($n = 2$).

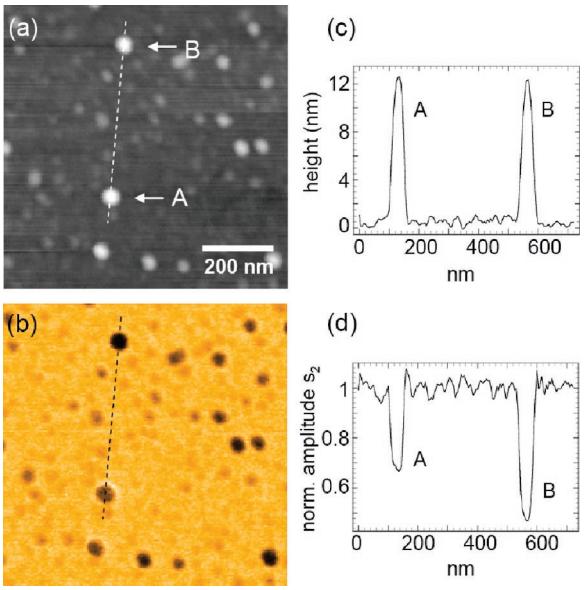

Figure 2. s-SNOM images of a binary mixture of Au and PS nanoparticles immobilized on a Si substrate. (a) Topography. (b) Simultaneously recorded optical signal amplitude s_2. (c) Line profile extracted along the dashed line in (a), showing the topography of two equally high particles A and B. (d) Line profile showing different optical signals s_2 for the two particles A and B.

and its mirror image in the sample, $p_t' = p_t\,(\epsilon - 1)/(\epsilon + 1)$, the interferometrically measured amplitude s_n and phase φ_n of the scattered light depend on the local dielectric function ϵ of the sample. The near-field optical images can thus be considered as dielectric maps of the sample surface where the spatial resolution is given by the size of the tip apex.[23,25] However, when probing nanoparticles smaller than the diameter of the tip apex, the interpretation of the near-field contrast is more complicated. Recently it was observed that the near-field contrast of nanoparticles depends on their size.[22,30] Even a size-dependent contrast reversal was reported.[30] Both observations can be described by an extended dipole model where the light scattered from the probe is calculated by considering the near-field interaction between a probe dipole p_t, a particle dipole p_p, and their corresponding mirror dipoles in the substrate (Figure 1b). In our model,[22] the nanoparticle dipole p_p is given by the polarizability α_p of a small sphere with diameter d and dielectric value ϵ_p, $\alpha_p = 4\pi(d/2)^3\,(\epsilon_p - 1)/(\epsilon_p + 2)$, while the probe dipole p_t is described by the polarizability α_t of a platinum ellipsoid with an apex radius of 20 nm and a dielectric value $\epsilon_t = -1000 + 500i$.

The extended dipole model is applied here to calculate the IR s-SNOM signal of nanoparticles dependent on the particle material. Figure 1c shows the results obtained for gold (Au, $\epsilon_p = -5000 + 1000i$) and polystyrene (PS, $\epsilon_p = 2.4 + 0.1i$) particles on a Si substrate ($\epsilon = 11.7$) at a wavelength $\lambda = 10.6\ \mu$m. We find stronger signal amplitudes s_2 for Au than for PS particles. More generally, for a given diameter d, we find an increasing signal amplitude s_2 when the dielectric values ϵ_p of the particle material increases (not shown). This can be explained by the increasing polarizability α_p of the particle, which enhances the strength of the particle dipole p_p. Below a particle size of about 1/3 of the tip radius, the particles cannot be distinguished anymore, as the coupling between the particle and the tip becomes negligible compared to the much stronger coupling between the tip and the substrate. However, from the graphs in Figure 1c, we predict that s-SNOM employing a Pt tip with radius of 20 nm should allow one to distinguish PS and Au particles with diameters d as small as 10 nm.

Experimentally, we demonstrate the material and size dependency of the s-SNOM contrast of nanoparticles by imaging colloidal Au and PS particles with diameters between 5 and 20 nm. The sample was prepared by immobilizing the particles on a flat Si surface covered by a 1−2 nm thick bovine serum albumin (BSA) film. A random distribution of the two particle types has been achieved by a two-step procedure. First, the substrate is exposed to a drop of colloidal Au nanoparticle solution for about 2 min. After drying the sample with nitrogen, the PS particles were adsorbed the same way. Near-field optical imaging was performed with our home-built infrared s-SNOM,[14] where a commercial Pt-coated Si tip (apex radius ≈ 20 nm) is illuminated by a focused CO_2 laser beam at a fixed wavelength $\lambda = 10.6\ \mu$m. Operating in tapping mode, the tip is vertically vibrating with an amplitude of 20 nm at a frequency $\Omega = 318$ kHz. Pseudoheterodyne interferometric detection and second harmonic (2 Ω) demodulation of the detector signal yield optical amplitude s_2 and phase φ_2 images simultaneously with topography.[31]

The topography of the nanoparticle mixture (Figure 2a) shows the homogeneous distribution of single nanoparticles

up to 20 nm in size. In the infrared near-field image (Figure 2b), we find that all particles (including the Au particles) appear darker than the Si substrate. By extracting line plots from the s-SNOM images, we can quantitatively compare near-field signal s_2 and particle diameter d. In the example shown in Figure 2, we find two particles of the same diameter (d = 12.8 nm, marked by A and B) that have different infrared signal amplitudes s_2. On particle B, the signal s_2 is about 30% lower than on A. Because the particles have equal sizes, this observation lets us conclude that the particles have different dielectric properties. As the particle mixture contains only Au and PS particles, we can identify A as a Au particle and B as a PS particle according to our calculation shown in Figure 1c.

We note that the negative near-field contrast of Au nanoparticles compared to the Si substrate (s_2(Au) < s_2(Si)) is different from the positive contrast (s_2(Au) > s_2(Si)) of extended Au nanostructures on a flat Si surface.[14,23,25−27] The latter is well established and explained by near-field coupling between the tip and its mirror image in the flat sample. When Au particles much smaller than the tip size are probed, the near-field coupling between the tip and the particle, as well as between the tip and the substrate, contribute to the signal amplitude s_2 (Figure 1b,c). When the vibrating tip follows the topography of a nanoparticle, the tip−substrate coupling decreases while a tip−particle coupling rises at the same time. However, the polarizability of small particles is obviously not strong enough to compensate the decreasing signal amplitude caused by the reduced tip−substrate coupling. The particle thus yields a reduced signal s_2 relative to the substrate. A similar observation was recently made with s-SNOM images of InGaN particles grown on a GaN substrate.[30]

We can demonstrate the size-dependent near-field optical material contrast of nanoparticles by correlating topography and near-field signal. This is done by plotting the optical signal amplitude $s_2(x,y)$ measured at a pixel (x,y) versus the height $h(x,y)$ extracted from the corresponding topography image. We exclude all pixels belonging to undefined structures and aggregates as well as pixels where the cantilever vibration amplitude differs by more than 2% from the average value obtained for the Si substrate. To minimize mechanically induced artifacts, i.e., the possibility that the near-field optical contrast between Au and PS particles is induced by the mechanical tip−particle interaction,[32] we further exclude all pixels where the mechanical phase of the cantilever vibration differs by more than 5° from the average value obtained on the Si substrate.

In Figure 3a, we show the result s_2 vs h, obtained by analyzing several s-SNOM images such as shown in Figure 2, which altogether cover a sample area of about 10 μm^2. Figure 3a reveals two distinct branches that can be separated from each other for h > 7 nm. In good qualitative agreement with our prediction (Figure 1c), we find that the s-SNOM signal of nanoparticles depends on both their size and dielectric constant. Clearly, the upper branch in Figure 3a can be assigned to Au particles and the lower branch to PS particles. To further verify this conclusion, we performed

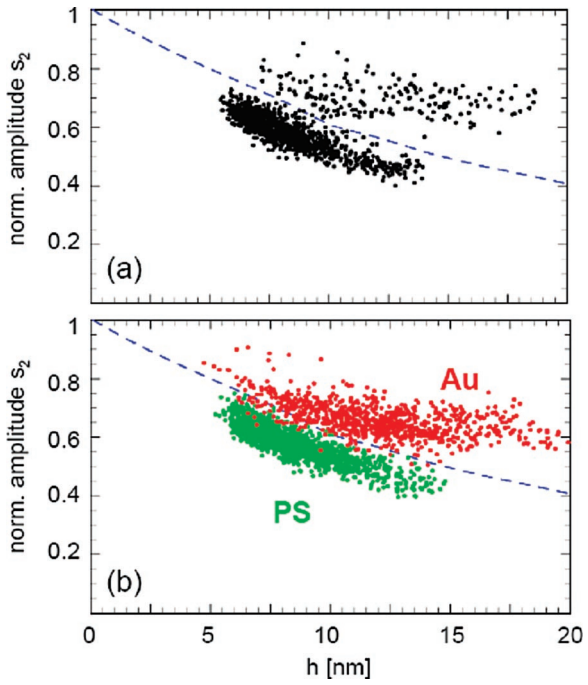

Figure 3. (a) Display of the near-field signal s_2 vs height h obtained from s-SNOM images of a sample where Au and PS nanoparticles are adsorbed on a Si substrate. (b) Results of control experiments where either Au (red data points) or PS (green data points) nanoparticles are adsorbed on a Si substrate. (a,b) All values are normalized to that of the Si substrate. The manually defined separator between Au and PS (dashed blue line, being the same in both graphs) is used to generate the material-specific maps shown in Figure 5a.

control experiments with samples where either Au or PS particles were adsorbed on a Si substrate. The two samples were imaged with the same tip and tip vibration amplitude as before. Employing subsequent data analysis as described above, we obtain $s_{2,Au}(h)$ for the Au sample (Figure 3b, red data points) and $s_{2,PS}(h)$ for the PS sample (Figure 3b, green data points). By comparison of the data sets (Figure 3a,b), we find a good agreement between $s_{2,Au}(h)$ and the upper branch in Figure 3a, while $s_{2,PS}(h)$ corresponds to the lower branch in Figure 3a.

In Figure 3, we observe significant fluctuations of the signal amplitude s_2. We assign them partly to the uncertainty in the height measurement caused by the inhomogeneous 1−2 nm thick BSA layer on the Si substrate. More importantly, our analysis does not take into account the position of the probe relative to the particle. The two experimental situations shown in Figure 4, for example, would yield data points in Figure 3 at the same height h. However, because of differences in the particle size and tip−particle geometry, we can expect a different optical near-field interaction between tip and sample, yielding variations in the optical signal s_2. More sophisticated image analysis taking into account the position of the tip relative to the particle might therefore reduce the signal fluctuations.

Obviously, the signal fluctuations play an important role for the material-specific differentiation of the nanoparticles. In our present experiments, we can successfully separate the near-field optical signals from Au and PS particles ≥7 nm

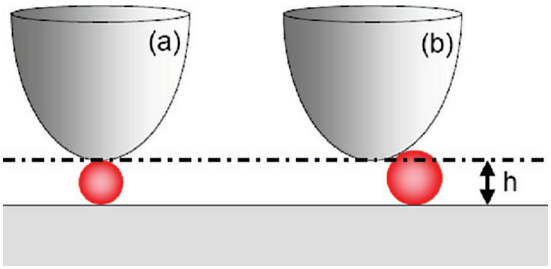

Figure 4. Two experimental situations yielding data points in Figure 3 at the same height *h*.

because of the strong difference in the dielectric properties of these materials, yielding only a minimal overlap of the two branches in Figure 3. For materials providing less dielectric contrast, we expect an increasing overlap of the branches, challenging an unambiguous material differentiation. In such a case, it will be crucial to reduce the signal fluctuations by improving the image analysis (see above) and by increasing the mechanical stability of the microscope setup. Note that any mechanical instability will generate noise in the near-field signal, which can be explained by the strongly distance-dependent near-field coupling between tip and sample.[22] However, noise reduction alone will not solve the fundamental problem arising with very small particles. As seen both in experiment (Figure 3) and theory (Figure 1c), the near-field contrast even between Au and PS is strongly decreasing for particles with $d < 7$ nm. As the particle dipole $p_p \propto d^3$ becomes negligible compared to the probe dipole p_t, the tip−substrate coupling dominates over the tip−particle coupling such that the near-field signal becomes insensitive to the dielectric properties of the particle.[22,30] According to the dipole model (Figure 1b), sharper tips would be beneficial to solve this problem, as the near-field optical contrast for a given particle size increases with decreasing tip radius.

A direct application of the results presented so far is demonstrated in Figure 5. With the aid of Figure 3a, we can generate material-specific maps of the analyzed particle mixture. For that purpose, in the topography images (Figure 5a), we color the pixels with $h(x,y) \geq 7$ nm according to whether they are located above (red) or below (green) the dashed blue line in Figure 3a. We have chosen this line manually in order to separate the two materials Au and PS. Because of the rigorous criteria (see above) underlying Figure 3a, only a few color pixels are found in Figure 5a. On the individual particles, all color pixels are found to be either red or green. This already verifies reliable material recognition on the single-particle level. To enhance the visibility of the particle color, we repeat our image analysis according to Figures 3 and 5a. But this time, we perform the analysis independent of the mechanical cantilever phase. We obtain Figure 5c, which yields significantly more color pixels. Intriguingly, the individual particles still appear either dominantly red or green. In the present case of Au and PS particles, changes in the mechanical tip−sample interaction obviously do not change the near-field optical material assignment for particles >7 nm. Considering also that our analysis is based on the correlation of single pixels rather than whole particles, the observed clustering of colored pixels is a remarkable result. Neither theoretical modeling nor sophisticated image analysis or processing is required to generate the color maps.

In conclusion, we demonstrated material-specific s-SNOM mapping of a binary mixture of Au and PS nanoparticles with successful recognition of particles down to 7 nm in diameter. We found that the near-field optical contrast of

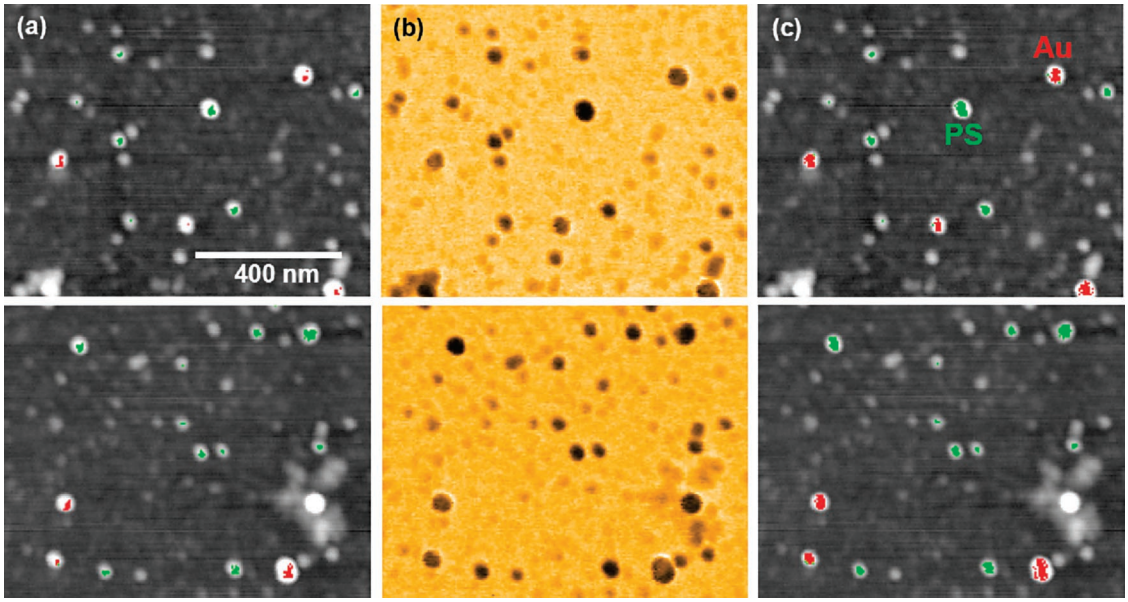

Figure 5. Two s-SNOM images of a mixture of Au and PS nanoparticles adsorbed on a Si substrate. The images show two different sample regions included in the analysis presented in Figure 3a. (a) Topography (gray scale). Single pixels measuring a height $h \geq 7$ nm are colored depending on whether the corresponding data points in Figure 3a are located above (red, Au) or below (green, PS) the material separator (dashed blue line). (b) Near-field optical signal amplitude s_2. (c) Material-specific maps generated analogous to (a) but now independent of the mechanical cantilever phase.

the particles depends on both their size and their dielectric properties, which can be described in a good approximation by an extended dipole model. By including higher multipoles and considering antenna effects in the probe, we expect to achieve a better quantitative description. Independent of theory, a simple analysis technique correlating topography and near-field image allows the separation of the two dependencies and enables the generation of material-specific maps of the particle mixture. Employing plasmon− or phonon−polariton-resonant tip−substrate coupling or sharper probe tips could push the limits of material-specific s-SNOM mapping even well below 5 nm particle size.[22] As near-field imaging can be performed at frequencies ranging from visible[14] to THz[33,34] and even microwave[35] frequencies, we expect interesting applications such as label-free near-field infrared mapping of protein complexes[18] in biomembranes, material-specific mapping of nanoparticle assemblies or recognition of conducting inclusions in nanocomposite materials. From the demonstrated possibility of s-SNOM to map free carriers in doped semiconductor nanostructures,[36,37] we also expect exciting studies of conduction properties in single sub-10 nm semiconductor crystals.

Acknowledgment. We thank R. Guckenberger, A. Huber, M. Brehm, N. Issa, and F. Keilmann (all Martinsried) for discussions and critical comments on the manuscript. Financial support by BMBF grant no. 03N8705 and the German Excellence Initiative via the "Nanosystems Initiative Munich (NIM)" is gratefully acknowledged.

References

(1) van Dijk, M. A.; Tchebotareva, A. L.; Orrit, M.; Lippitz, M.; Berciaud, S.; Lasne, D.; Cognet, L.; Lounis, B. *Phys. Chem. Chem. Phys.* **2006**, *8*, 3486−3495.
(2) Lindfors, K.; Kalkbrenner, T.; Stoller, P.; Sandoghdar, V. *Phys. Rev. Lett.* **2004**, *93*, 037401.
(3) Ignatovich, F. V.; Novotny, L. *Phys. Rev. Lett.* **2006**, *96*, *139011*.
(4) Boyer, D.; Tamarat, P.; Maali, A.; Lounis, B.; Orrit, M. Science **2002**, *297*, 1160−1163.
(5) Muhlschlegel, P.; Eisler, H. J.; Martin, O. J. F.; Hecht, B.; Pohl, D. W. *Science* **2005**, *308*, 1607−1609.
(6) Schuck, P. J.; Fromm, D. P.; Sundaramurthy, A.; Kino, G. S.; Moerner, W. E. *Phys. Rev. Lett.* **2005**, *94*, 017402.
(7) Novotny, L. *Phys. Rev. Lett.* **2007**, *98*, 266802.
(8) Kalkbrenner, T.; Hakanson, U.; Schadle, A.; Burger, S.; Henkel, C.; Sandoghdar, V. *Phys. Rev. Lett.* **2005**, *95*, 200801.
(9) Anger P.; Bharadwaj P.; Novotny L. *Phys. Rev. Lett.* **2006**, *96*, *113002*.
(10) Kim, Z. H.; Leone S. R. *J. Phys. Chem. B* **2006**, *110*, 19804−19809.
(11) Inouye, Y.; Kawata, S. *Opt. Lett.* **1994**, *19*, 159−161.
(12) Lahrech, A.; Bachelot, R.; Gleyzes, P.; Boccara, A. C. *Opt. Lett.* **1996**, *21*, 1315−1317.
(13) Frey, H. G.; Witt, S.; Felderer, K.; Guckenberger, R. *Phys. Rev. Lett.* **2004**, *93*, 200801.
(14) Keilmann, F.; Hillenbrand, R. *Phil. Trans. R. Soc. London, Ser. A* **2004**, *362*, 787−805.
(15) Hartschuh, A.; Beversluis, M. R.; Bouhelier, A.; Novotny, L. *Phil. Trans. R. Soc. London, Ser. A* **2004**, *362*, 807−819.
(16) Gerton, J. M.; Wade, L. A.; Lessard, G. A.; Ma, Z.; Quake, S. R. *Phys. Rev. Lett.* **2004**, *93*, 180801.
(17) Hartschuh, A.; Sanchez, E. J.; Xie, X. S.; Novotny, L. *Phys. Rev. Lett.* **2003**, *90*, 955031−955034.
(18) Brehm, M.; Taubner, T.; Hillenbrand, R.; Keilmann, F. *Nano Lett.* **2006**, *6*, 1307−1310.
(19) Pettinger, B.; Ren, B.; Picardi, G.; Schuster, R.; Ertl, G. *Phys. Rev. Lett.* **2004**, *92*, 961011−961014.
(20) Neacsu, C. C.; Dreyer, J.; Behr, N.; Raschke, M. B. *Phys. Rev. B* **2006**, *73*, 193406.
(21) Rasmussen, A.; Deckert, V. *J. Raman Spectrosc.* **2006**, *37*, 311−317.
(22) Cvitkovic, A.; Ocelic, N.; Aizpurua, J.; Guckenberger, R.; Hillenbrand, R. *Phys. Rev. Lett.* **2006**, *97*, 060801.
(23) Hillenbrand, R.; Keilmann, F. *Appl. Phys. Lett.* **2002**, *80*, 25−27.
(24) Hillenbrand, R.; Taubner, T.; Keilmann, F. *Nature* **2002**, *418*, 159−162.
(25) Taubner, T.; Hillenbrand, R.; Keilmann, F. *J. Microsc.* **2003**, *210*, 311−314.
(26) Raschke, M. B.; Lienau, C. *Appl. Phys. Lett.* **2003**, *83*, 5089−5091.
(27) Bek, A.; Vogelgesang, R.; Kern, K. *Rev. Sci. Instrum.* **2006**, *77*, 043703.
(28) Knoll, B.; Keilmann, F. *Opt. Commun.* **2000**, *182*, 321−328.
(29) Hillenbrand, R.; Keilmann, F. *Phys. Rev. Lett.* **2000**, *85*, 3029−3032.
(30) Kim, Z. H.; Ahn, S.-H.; Liu, B.; Leone, S. R. *Nano Lett.* **2007**, *7*, 2258−2262.
(31) Ocelic, N.; Huber, A.; Hillenbrand, R. *Appl. Phys. Lett.* **2006**, *89*, 101124.
(32) Bek, A.; Vogelgesang, R.; Kern, K. *Appl. Phys. Lett.* **2005**, *87*, 163115.
(33) Rosner, B. T.; van der Weide, D. W. *Rev. Sci. Instrum.* **2002**, *73*, 2505−2525.
(34) Chen, H.-T.; Kraatz, S.; Kersting, R.; Cho, G. C. *Phys. Rev. Lett.* **2004**, *93*, 267401.
(35) Knoll, B.; Keilmann, F.; Kramer, A.; Guckenberger, R. *Appl. Phys. Lett.* **1997**, *70*, 2667.
(36) Knoll, B.; Keilmann, F. *Appl. Phys. Lett.* **2000**, *77*, 3980.
(37) Huber, A. J.; Kazantsev, D.; Keilmann, F.; Wittborn, J.; Hillenbrand, R. *Adv. Mater.* **2007**, *19*, 2209−2212.

NL071775+